

THESIS

EFFICIENCY MODELING FOR NEUTRON DETECTORS

Submitted by

Lisa Marie Scallan

Department of Environmental and Radiological Health Sciences

In partial fulfillment of the requirements

For the Degree of Master of Science

Colorado State University

Fort Collins, Colorado

Summer 2014

Master's Committee:

Advisor: Alex Brandl

Thomas Johnson  
Suren Chen

Copyright by Lisa Marie Scallan 2014

All Rights Reserved

## ABSTRACT

### EFFICIENCY MODELING FOR NEUTRON DETECTORS

Neutron detectors are used for various applications, such as for workplace monitoring in a neutron field, during nuclear incidents, and for the detection of contraband nuclear material. The Remote Sensing Laboratory has developed and employed several neutron detector designs, and characterization data have been collected with these detectors under varying environmental conditions. Using MCNP/MCNPX the neutron fluence rate and dose rate were evaluated during open-field deployment as a function of moisture content in air and soil, barometric pressure, and varying pavement and soil composition. The focus of this analysis was on the incident neutron spectra, detector efficiency and count rate at the detector location. The most prevalent parameters directly contributing to scattered neutrons into the active detector volume were evaluated. Experimentally observed functional dependence on the source-detector distance was compared to MCNP/MCNPX simulation data. This study provides detector efficiency data for a wide range of operational conditions beyond the current capacity for experimental detector characterization.

## TABLE OF CONTENTS

ABSTRACT.....	ii
LIST OF TABLES.....	iv
LIST OF FIGURES.....	v
INTRODUCTION, THEORY AND BACKGROUND.....	1
MATERIALS AND METHODS.....	8
RESULTS.....	15
DISCUSSION.....	24
CONCLUSION.....	27
REFERENCES.....	28
APPENDIX I.....	29
APPENDIX II.....	31
APPENDIX III.....	32
APPENDIX IV.....	33
APPENDIX V.....	34
APPENDIX VI.....	35
APPENDIX VII.....	36

## LIST OF TABLES

Table 1. Summary of interaction probabilities for typical Helium-3 and Boron-10 detectors (Crane, T.W. and Baker, M.P., 1991).....	3
Table 2. Summary of materials used for neutron detection (Knoll, 2010) .....	4
Table 3. Weather data for sampling in open air over asphalt (Remote Sensing Laboratory).....	10
Table 4. Ideal bulk densities for three types of soil (USDA Natural Resources Conservation Service, 2008) .....	12
Table 5. Summary of soil moisture data from three locations (European Space Agency, 2012).	13
Table 6. Densities used to evaluate asphalt and concrete using MCNPX .....	13
Table 7. Values of Barometric Pressure and Relative Humidity evaluated with MCNPX .....	14
Table 8. Summary of detectors evaluated.....	15
Table 9. Comparison to “1/R <sup>2</sup> Law” .....	23
Table 10. MCNPX modeling data for Detector B .....	23
Table 11. Comparison to “1/R <sup>2</sup> Law” with Detector and Source Moderation for Detector B Experimental Results .....	23
Table 12. Comparison to “1/R <sup>2</sup> Law” with Source Moderation for Detector C Experimental Results.....	23

## LIST OF FIGURES

Figure 1. Energy distribution of fission neutrons (Cember, 2009).....	2
Figure 2. Cross section versus neutron energy (Knoll, 2010).....	4
Figure 3. Expected pulse height spectrum with significant wall effect for Helium-3 tube (Knoll, 2010).....	6
Figure 4. Neutron detector operation (United States Government Accountability Office, 2011)....	6
Figure 5. Cross-section view of Detector C geometry; Helium-3 tube (1), moderator (2) (Remote Sensing Laboratory).....	9
Figure 6. 3D view of Detector E.....	9
Figure 7. Data collection setup; the Californium-252 source (circled) is on the left inside a white HDPE cylinder, the backpack on the right contains a neutron detector (Remote Sensing Laboratory) .....	11
Figure 8. Californium-252 spontaneous fission source neutron spectrum (International Standard (ISO/DIS 8529-1), 2000) .....	11
Figure 9. Soil Moisture Monthly Mean for July 2008. Data collection locations: 1. Phoenix, Arizona; 2. Syracuse, New York (European Space Agency, 2012) .....	13
Figure 10. Detector B: Experimental data (triangles) compared with MCNPX modeling (squares) with varying source-detector distances over soil .....	16
Figure 11. Detector B: Experimental data (triangles) compared with MCNPX modeling (squares) with varying source-detector distances over asphalt .....	16
Figure 12. Detector C: Experimental data (triangles) compared with MCNPX modeling (squares) with varying source-detector distances over soil .....	17
Figure 13. Detector C: Experimental data (triangles) compared with MCNPX modeling (squares) with varying source-detector distances over asphalt .....	17
Figure 14. Results of MCNPX modeling with varying ground moisture .....	18
Figure 15. Results of MCNPX modeling with varying air moisture .....	19
Figure 16. Results of MCNPX modeling with varying barometric pressure.....	19
Figure 17. Results of MCNPX modeling with varying ground type for complex detectors .....	20
Figure 18. Results of MCNPX modeling with varying ground type for simple detectors .....	20
Figure 19. Comparison of effects of ground type for experimental data.....	21
Figure 20. Results of MCNPX modeling with varying source-detector distance over soil.....	22
Figure 21. Results of MCNPX modeling with varying source-detector distance over asphalt ....	22

## INTRODUCTION, THEORY AND BACKGROUND

Due to changes throughout the world in the last decade, radiation detection devices have become increasingly important in maintaining national security. Specifically, neutron detectors are of importance because of their ability to detect small amounts of nuclear contraband or fission products that could be used in hostile actions. Neutron detectors range from small, mobile systems used by foot patrols to large, permanent systems at border crossings and exits of nuclear facilities. Since immediate results are usually necessary, these detectors are required to provide accurate, real-time information.

Due to national security uses of neutron detectors, the timing and location of when they are required to operate are usually not known. Therefore, the environmental and physical conditions of the area, which may impact detector measurements, can also be unknowns. To ensure experimental measurements are accurately interpreted, it is crucial to have advanced understanding of how environmental and physical variables affect neutron detector outputs.

Neutron background information, including energy dependence at ground level, is required to accurately measure neutrons in the environment (Ide, 2012). Environmental factors could affect the background neutron count rate, however, no straightforward relationship between temperature, humidity, or pressure and the neutron count rate can be concluded (Ide, 2012). Neutrons with energies approximately between 0.1 MeV and 20 MeV are considered fast neutrons while neutrons with energies less than 0.025 eV are known as thermal neutrons (Turner, 2007). As seen in Figure 1, fission neutrons caused by the splitting of a nucleus range in energies with an average energy of 2 MeV (Cember, 2009). With the exception of very short lived fission fragments, radionuclides do not decay by emitting neutrons (Cember, 2009). The neutron fluence rate from rocks measured at 1,070 meters underground was estimated as  $1.72 \times 10^{-6} \text{ cm}^{-2}\text{s}^{-1}$

above 0.5 MeV (Tziaferi, 2007). Approximately 268 meters above ground, an average neutron fluence rate of  $4 \times 10^{-4} \text{ cm}^{-2}\text{s}^{-1}$  has been measured below 6 MeV which is the region of interest for nuclear non-proliferation and safeguards applications (Ide, 2012). The below ground neutron fluence rate is two orders of magnitude smaller than the neutron fluence rate measured near sea level, indicating neutron production by cosmic radiation is more prevalent than terrestrial sources at the energies of interest.

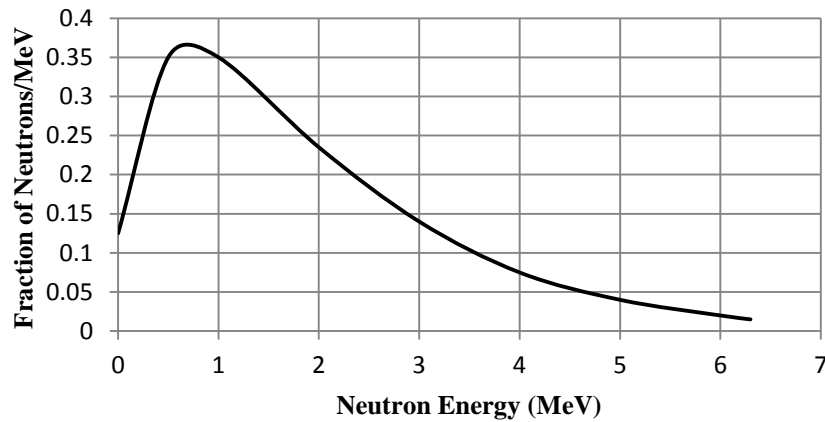


Figure 1. Energy distribution of fission neutrons (Cember, 2009)

Detecting fast neutrons for nuclear non-proliferation and nuclear safeguards applications is advantageous because of the relatively rare abundance of fast neutrons in a typical radiation background (Ide, 2012). Therefore, if neutrons are found, even at low levels, the source should be investigated. Additionally, neutrons are hard for perpetrators to shield, unlike gamma rays that can be shielded by high atomic number (high-Z) materials.

Challenges when detecting neutron radiation include eliminating interferences from background radiation, specifically gamma radiation, and assuring the detector material is abundantly available in nature or easily and cost effectively produced. Also, the target material in a detector requires a large cross section, thus relatively high probability of interaction, to ensure

a reaction occurs in the smallest amount of space to reduce detector size. Boron-10, Lithium-6 and Helium-3 are common isotopes used in neutron detectors.

Gamma rays may be present at levels ten times greater than neutrons when surveying nuclear materials; therefore, gamma suppression is one of the main considerations in choosing neutron detectors (Crane, T.W. and Baker, M.P., 1991). Helium-3 detectors provide good gamma radiation suppression because of the low interaction probability for gamma rays compared to the interaction probability for thermal neutrons, thus eliminating false positives caused by gammas (Crane, T.W. and Baker, M.P., 1991). As shown in Table 1, fewer background gamma interactions and more neutron interactions are detected using detectors with Helium-3, which is a significant advantage over Boron-10 detectors.

**Table 1. Summary of interaction probabilities for typical Helium-3 and Boron-10 detectors (Crane, T.W. and Baker, M.P., 1991)**

Thermal Detectors	Interaction Probability	
	Thermal Neutron	1-MeV Gamma Ray
<b>3He (2.5 cm diam, 4 atm)</b>	0.77	0.0001
<b>BF3 (5.0 cm diam, 0.66 atm)</b>	0.29	0.0006

Naturally occurring Helium-3 is very rare, and today most Helium-3 is produced from the radioactive decay of tritium. In the past, tritium was produced to support the United States nuclear weapons program. The National Nuclear Security Administration currently maintains the tritium stockpile and, therefore, the most abundant Helium-3 supply. As more Helium-3 neutron detectors were produced, the demand for Helium-3 increased. A shortage of Helium-3 was identified by the U.S. Government in 2008, however, Department of Homeland Security (DHS) reported supplies of Boron-10 and Lithium-6 are sufficient for future requirements. Both isotopes have a higher natural abundance than Helium-3 (United States Government Accountability Office, 2011).

As shown in Table 2, Helium-3 has the highest cross section for detecting thermal neutrons, which is an advantage over other elements. The cross section is expressed in units of area, traditionally known as a barn (b). The cross section decreases as energy increases (Figure 2), therefore, it is important the neutrons are thermalized before being detected using Helium-3. Helium-3 is also a good option because it is non-toxic and non-radioactive ensuring no interference from natural radiation in the detection material. Large numbers of Boron-10, Lithium-6, and Helium-3 neutron detectors are being used today because of their ability to detect neutrons. However, Helium-3 has many properties making it an ideal isotope for the light-weight, mobile neutron detectors required for Homeland Security uses.

**Table 2. Summary of materials used for neutron detection (Knoll, 2010)**

Element	Reaction Type	Thermal Neutron Cross Section (b)
<b>Helium-3</b>	n,p	5330
<b>Lithium-6</b>	n, $\alpha$	940
<b>Boron-10</b>	n, $\alpha$	3840

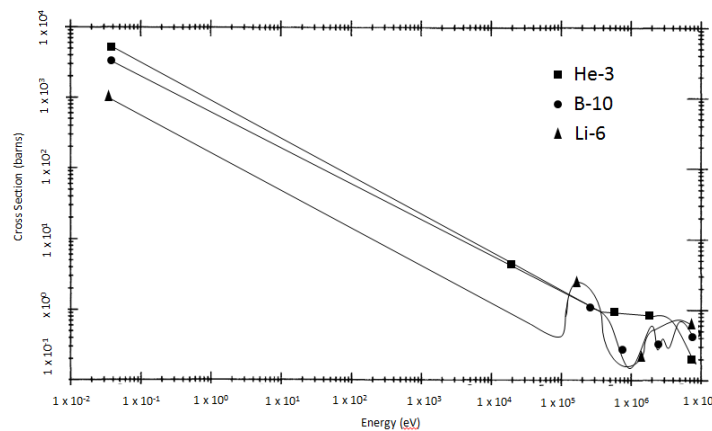


**Figure 2. Cross section versus neutron energy (Knoll, 2010)**

Neutrons can be difficult to detect because they do not carry electric charge and unlike gamma rays, neutrons do not interact directly with electrons in matter. Therefore, a reaction that

produces a charged particle is required in neutron detection. Detecting thermal neutrons in Helium-3 detectors is possible because of Equation 1,



in which the Helium-3 nucleus becomes unstable following a neutron interaction and breaks up into a tritium nucleus and a proton. The two charged particles share the 764 keV reaction energy (proton: 573 keV and triton: 191 keV) which is very large compared to the energy of the incoming neutron (Knoll, 2010).

Helium-3 is usually used as the fill gas in a proportional counter (Knoll, 2010). The proton and triton ionize the Helium-3 gas as they slow down and stop, which creates electron-ion pairs. Since both particles are emitted in opposite directions, one or the other should be detected (Crane, T.W. and Baker, M.P., 1991).

As the ion pairs drift toward the anode they gain enough energy to ionize additional atoms, creating an electron avalanche. The electrons are collected as an electrical signal and converted to an analog pulse signal. This signal is directly proportional to the number of electrons formed in the avalanche which is directly proportional the number of primary ion pairs. Therefore, the pulse signal produced by the detector is directly proportional to the incident neutron radiation reacting with the gas (D. Mazed, 2012). However, since fast neutrons are moderated before entering the detector, all information regarding the initial neutron energy is lost. Fast neutrons are moderated with a low atomic number (low-Z) material, such as water or plastic, to become thermal neutrons that can be detected. Using different thicknesses of moderators allows neutron spectral data to be collected.

The neutron detection efficiency varies with the pressure of the Helium-3 gas and the dimensions of the detector (D. Mazed, 2012). Because Helium-3 has a low atomic mass, the

ranges of the reaction products are considerably long. Therefore, not all of the energy from the ionization events is deposited in the gas, creating a wall effect. If either the proton or the triton hits the wall, a smaller pulse is created. To decrease wall effects, the pressure of the fill gas or the diameter of the Helium-3 tubes can be increased. The expected pulse height spectrum in a typical Helium-3 tube with a significant wall effect is shown in Figure 3 (Knoll, 2010).

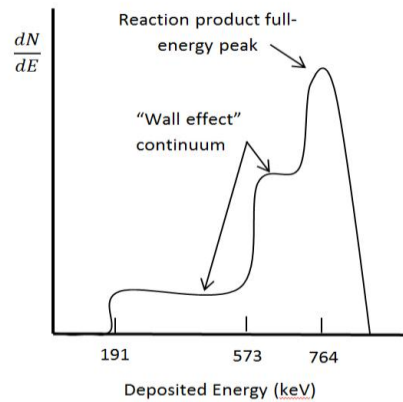


**Figure 3. Expected pulse height spectrum with significant wall effect for Helium-3 tube (Knoll, 2010)**

A summary of neutron detection can be seen in Figure 4.

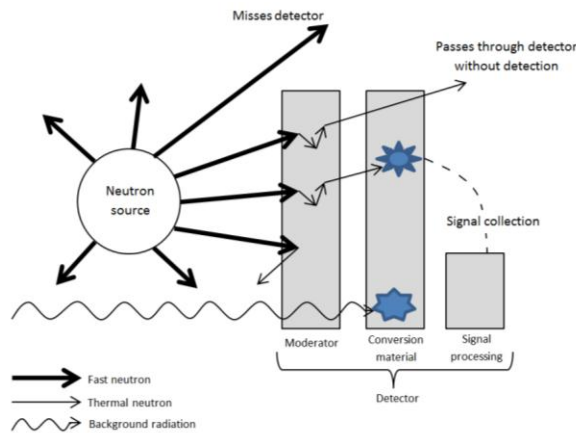


**Figure 4. Neutron detector operation (United States Government Accountability Office, 2011)**

Collecting and evaluating data from neutron detectors can be very time consuming and monotonous. Numerous variables including environmental factors and distances and geometries of the detector can impact detector readings. Therefore, the most efficient way to predict neutron detector responses is to model the output using computer code where variables can quickly be

changed and re-evaluated. The data collected from the computer model requires validation by comparison with experimental data.

## MATERIALS AND METHODS

During response scenarios, the variables of the sampling environment are almost always unknown, and quick, accurate results are required. Therefore, the most efficient and safe way to predict radiation dose is to model the scenario using computer codes where variables can quickly be changed and re-evaluated. An effective method is using Monte Carlo calculations, specifically Monte Carlo N-Particle Transport (MCNPX) code, to model radiation transport. Radiation emissions and interactions are natural stochastic events that are unpredictable at a single interaction level. Monte Carlo calculations employ games of chance or random sampling to follow the life history of particles and can produce results such as surface fluence, radiation dose, and energy spectra. A neutron can be followed from birth at a random position, direction, and time until termination such as absorption (Kalos, 2008). By comparing experimental measurements to modeling outputs obtained from MCNP, predetermined calibration factors can be identified.

Using single Helium-3 tubes, there are numerous options for designing detectors. Five geometries have been evaluated using MCNPX; three complex geometries of experimental detectors and two simple geometries to evaluate the impact of circuitry and other system components to the MCNP output. The first complex geometry evaluated was Detector A, comprised of 1-inch diameter Helium-3 tubes as well as a sodium iodide (NaI) crystal for gamma ray detection. Detector B consists of an array of 2-inch diameter Helium-3 tubes and other system components. The final complex geometry analyzed, Detector C, includes one 2-inch diameter Helium-3 tube embedded in a cylindrical shell of 3.81-inch high-density polyethylene (HDPE) as shown in Figure 5 (Remote Sensing Laboratory). The first simple geometry was

Detector D consisting of one Helium-3 tube inside simple casing. The second simple geometry, Detector E shown in Figure 6, was a five Helium-3 tube array.

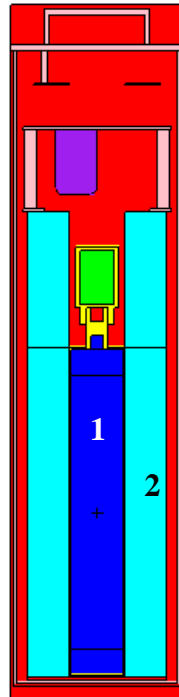


Figure 5. Cross-section view of Detector C geometry; Helium-3 tube (1), moderator (2) (Remote Sensing Laboratory)

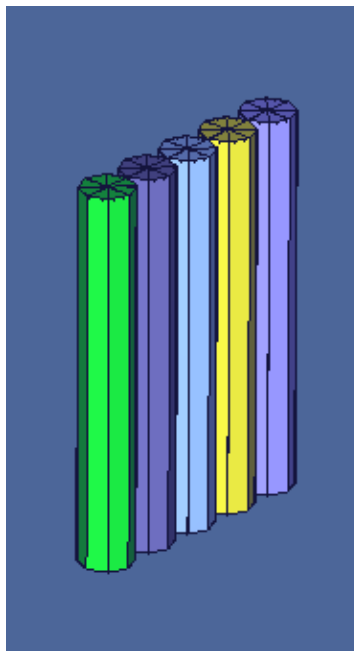


Figure 6. 3D view of Detector E

The neutron detector systems described above were used to collect background and neutron source response data using a Californium-252 source at the Remote Sensing Laboratory on Joint Base Andrews, Maryland. Data were collected in an open grass lot on 14 June 2012 and in an empty asphalt parking lot from 26 to 27 March 2012; detectors were positioned one meter above the ground. Specific weather data for all measurements are summarized in **Table 3**. The neutron count rate was recorded every 5 meters from 5 to 50 meters from the source to evaluate the relationship between the source and detector distances. All data were collected for greater than 400 total counts (Remote Sensing Laboratory). Since the detectors require the neutrons to be thermalized, experimental data was collected in two arrangements, bare and inside 1-inch HDPE. These arrangements provide information for fast and thermal neutrons, including the percent of thermal neutrons shielded by HDPE.

**Table 3. Weather data for sampling in open air over asphalt (Remote Sensing Laboratory)**

<b>Date/Time</b>	<b>Atmospheric Pressure (mbar)</b>			<b>Relative Humidity (%)</b>		
	0800 hrs	1200 hrs	1600 hrs	Minimum	Maximum	Average
<b>26 Mar 2012</b>	1010	1013	1014	24	88	49
<b>27 Mar 2012</b>	1028	1027	1025	19	56	34
<b>Average</b>	1019	1020	1019.5	21.5	72	41.5

The initial activity ( $A_0$ ) of the source, the Californium-252 decay constant ( $\lambda$ ) and time elapsed since source creation ( $t$ ), were used in Equation 2,

$$A_{(t)} = A_0 e^{-\lambda t}, \quad (2)$$

to calculate the activity of the source at the time of data collection ( $A_{(t)}$ ). With an initial activity of 500  $\mu\text{Ci}$  on 15 July 2006, the Californium-252 source used to collect data had a calculated activity of 112.3  $\mu\text{Ci}$  on 26 March 2012 and 106.0  $\mu\text{Ci}$  on 14 June 2012; Californium-252 has a relatively short half-life of 2.645 years. The Californium-252 source was placed on a tripod, one meter above the ground for all measurements as shown in Figure 7 (Remote Sensing Laboratory). Data were collected with the bare source and using 1.75-inch HDPE to moderate



Soil moisture and type are two environmental variables that have the potential to influence measurements by neutron detectors; the effects of these variables on detector response were evaluated using MCNPX. A cell card was created to simulate soil located one meter below the neutron detector. Three types of soils with varying bulk densities were evaluated (Table 4).

**Table 4. Ideal bulk densities for three types of soil (USDA Natural Resources Conservation Service, 2008)**

<b>Soil Type</b>	<b>Ideal bulk densities for plant growth (g/cm<sup>3</sup>)</b>
<b>Sandy</b>	1.60
<b>Silty</b>	1.40
<b>Clayey</b>	1.10

To evaluate the impact of soil moisture on the sensitivity of neutron detectors, data from three locations across the United States were obtained and evaluated. The first sampling location, Phoenix, Arizona, was chosen as the extreme dry location while Syracuse, New York was chosen as the extreme moist location. Soil moisture data were obtained from the European Space Agency’s (ESA) Climate Change Initiative Soil Moisture project. The project merged active and passive sampling data from microwave sensors to produce a soil moisture seasonality map (Figure 9); soil moisture is expressed as volumetric soil moisture (m<sup>3</sup>/m<sup>3</sup>). Soil moisture levels were collected at each location one time per month with the exception of times when the soil was frozen or covered with snow. Data are provided from 1979 to 2010, however, for this thesis, only data from 2004 to 2010 are evaluated (13). The average and range of soil moisture from the two locations are summarized in Table 5. Material composition of each type of soil was obtained and is summarized in Appendix II (Pacific Northwest National Laboratory, 2011). The chemical composition and soil moisture data of the three soil types were used to create the material cards for the MCNPX analysis; the endf70a neutron cross-section data library was used to provide cross-section data for the various neutron interactions in the different soils. Additionally,

MCNPX was used to model neutron detector response over asphalt and concrete using the density shown in Table 6 and the composition fractions shown in Appendix III.

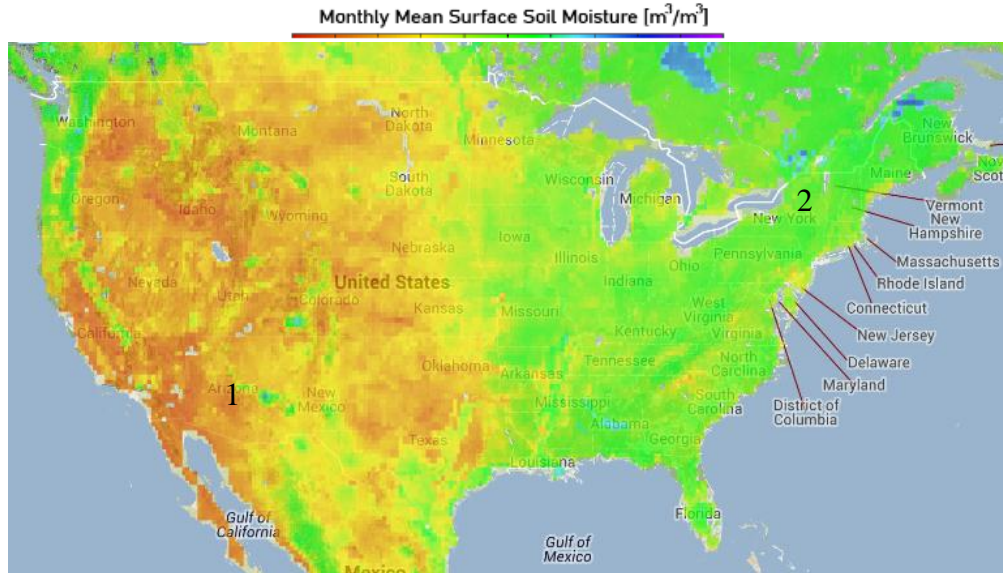


Figure 9. Soil Moisture Monthly Mean for July 2008. Data collection locations: 1. Phoenix, Arizona; 2. Syracuse, New York (European Space Agency, 2012)

Table 5. Summary of soil moisture data from three locations (European Space Agency, 2012)

Sampling Location	Average Soil Moisture ( $m^3/m^3$ )	Soil Moisture Range ( $m^3/m^3$ )
Phoenix, Arizona	0.09	0.05 - 0.21
Syracuse, New York	0.27	0.22 - 0.31

Table 6. Densities used to evaluate asphalt and concrete using MCNPX

Material	Density ( $g/cm^3$ )
Asphalt	1.30
Concrete, Los Alamos (MCNP)	2.25

The effects of relative humidity and barometric pressure on the neutron detectors were also evaluated using MCNPX. As elevation increases, the barometric pressure and density of the air decreases. Effects of barometric pressure were evaluated at three elevations by varying air density, as seen in Table 7; temperature was assumed to be 20°C and relative humidity levels were assumed to be 50%. The effects of relative humidity, as a function of water content in the air, were also evaluated at three different levels, as seen in Table 7 (Bahadori, 2011). The effects

of the environmental variables were determined by changing one variable per MCNP input, while keeping all other variables constant.

**Table 7. Values of Barometric Pressure and Relative Humidity evaluated with MCNPX**

<b>Elevation (m)</b>	<b>Barometric Pressure (hPa)</b>	<b>Air Density (kg/m<sup>3</sup>)</b>	<b>Relative Humidity (%)</b>	<b>Water Content (mL/m<sup>3</sup>)</b>
0	1010	1.195	5	2
800	918	1.086	50	9
1609	832	0.984	100	18

To decrease MCNPX computing time and uncertainty, up to ten of the same detectors and variables were analyzed at once. Equations 3 and 4,

$$\mu' = \frac{\sum\left(\frac{x_i}{\sigma_i^2}\right)}{\sum\left(\frac{1}{\sigma_i^2}\right)} \quad (3)$$

$$\sigma_{\mu}^2 = \frac{1}{\sum\left(\frac{1}{\sigma_i^2}\right)} \quad (4)$$

were used to calculate an overall mean ( $\mu'$ ) and standard deviation ( $\sigma_{\mu}$ ), where  $x_i$  and  $\sigma_i$  were the means and standard deviations of the individual Monte Carlo outputs, respectively (Bevington, 2003).

## RESULTS

Results from MCNPX were compared to experimental data to ensure the modeled outputs were accurately interpreted. A summary of the detectors evaluated and how they are labeled is shown in Table 8. The comparison of experimental and modeled count rates with varying source-detector distances on soil and asphalt is shown in Figures 10 through 13.

**Table 8. Summary of detectors evaluated**

<b>Detector Label</b>	<b>Data Source</b>	<b>Detector Description</b>
<b>Detector A</b>	MCNPX modeling	1-inch diameter Helium-3 tubes, sodium iodide (NaI) crystal
<b>Experimental Detector B</b>	Experimental	Array of 2-inch diameter Helium-3 tubes
<b>Detector B</b>	MCNPX modeling	One 2-inch diameter Helium-3 tube embedded in cylindrical shell of 3.81-inch (HDPE)
<b>Experimental Detector C</b>	Experimental	One Helium-3 tube
<b>Detector C</b>	MCNPX modeling	Five Helium-3 tube array
<b>Detector D</b>	MCNPX modeling	
<b>Detector E</b>	MCNPX modeling	

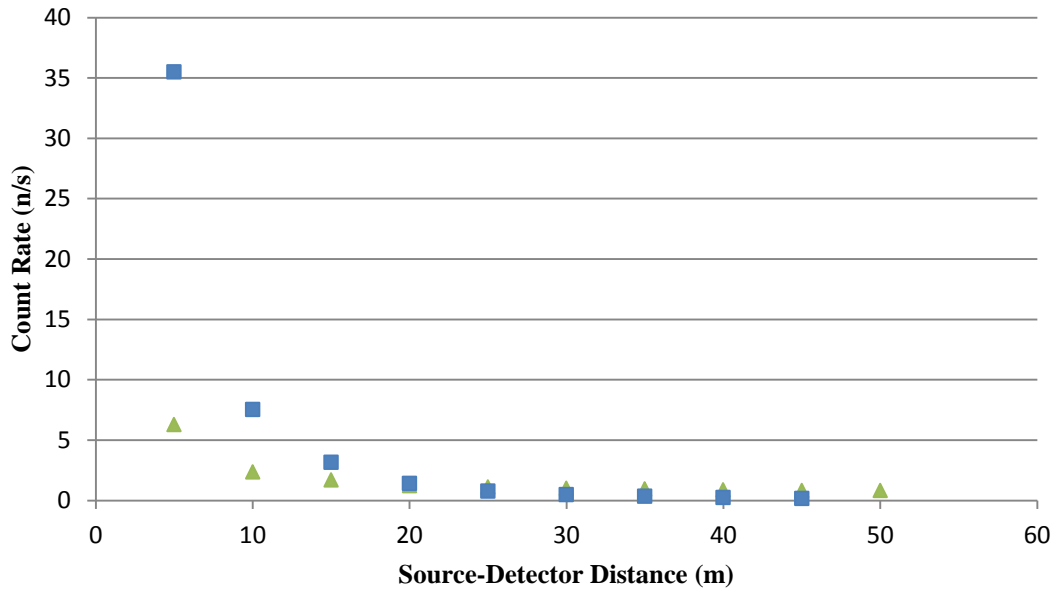


Figure 10. Detector B: Experimental data (triangles) compared with MCNPX modeling (squares) with varying source-detector distances over soil

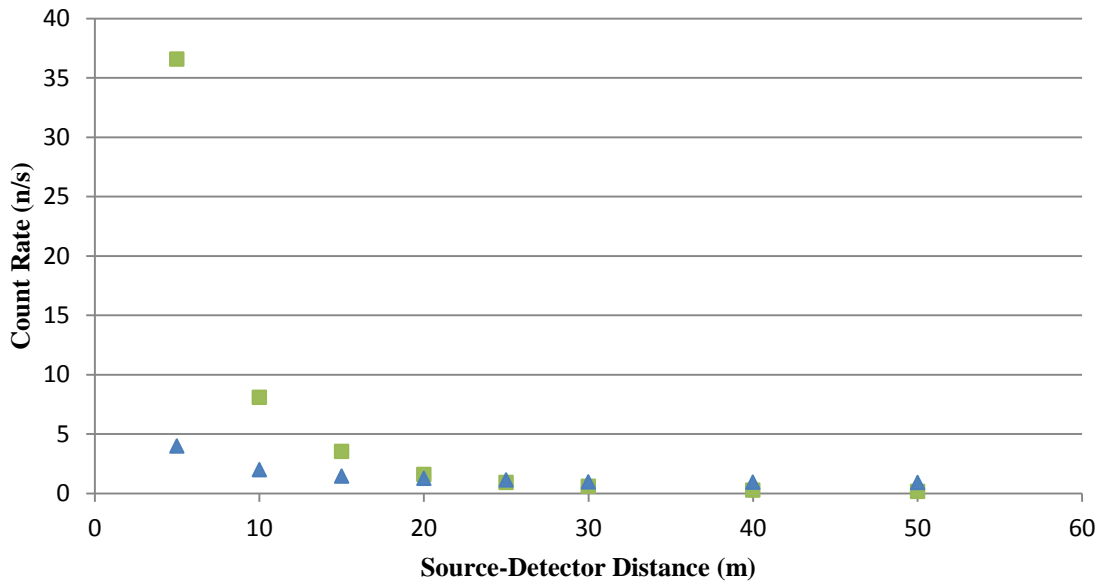


Figure 11. Detector B: Experimental data (triangles) compared with MCNPX modeling (squares) with varying source-detector distances over asphalt

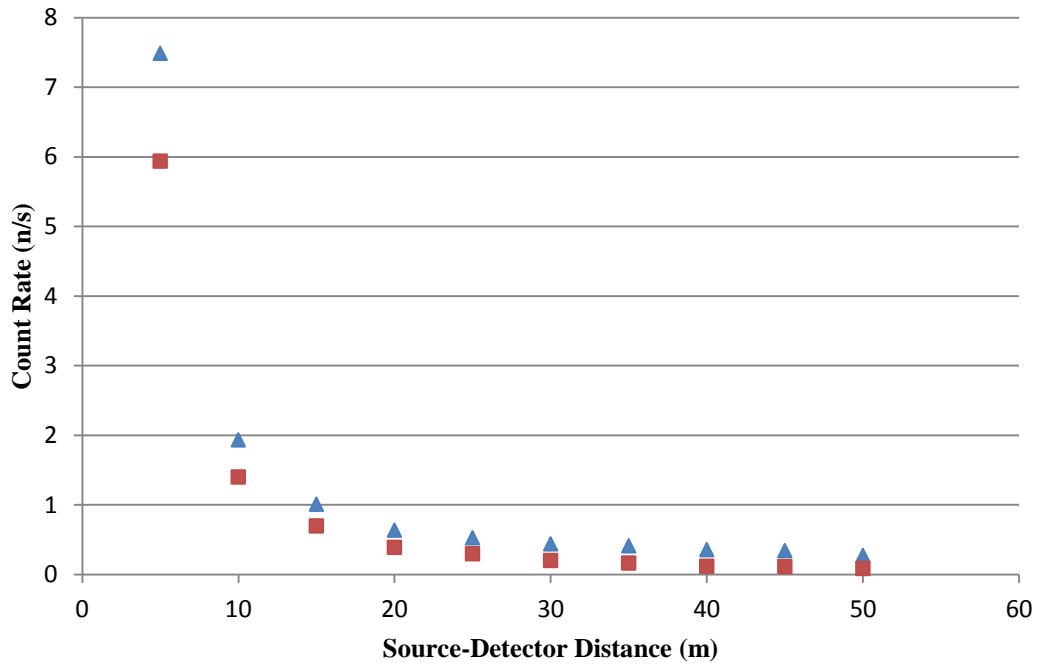


Figure 12. Detector C: Experimental data (triangles) compared with MCNPX modeling (squares) with varying source-detector distances over soil

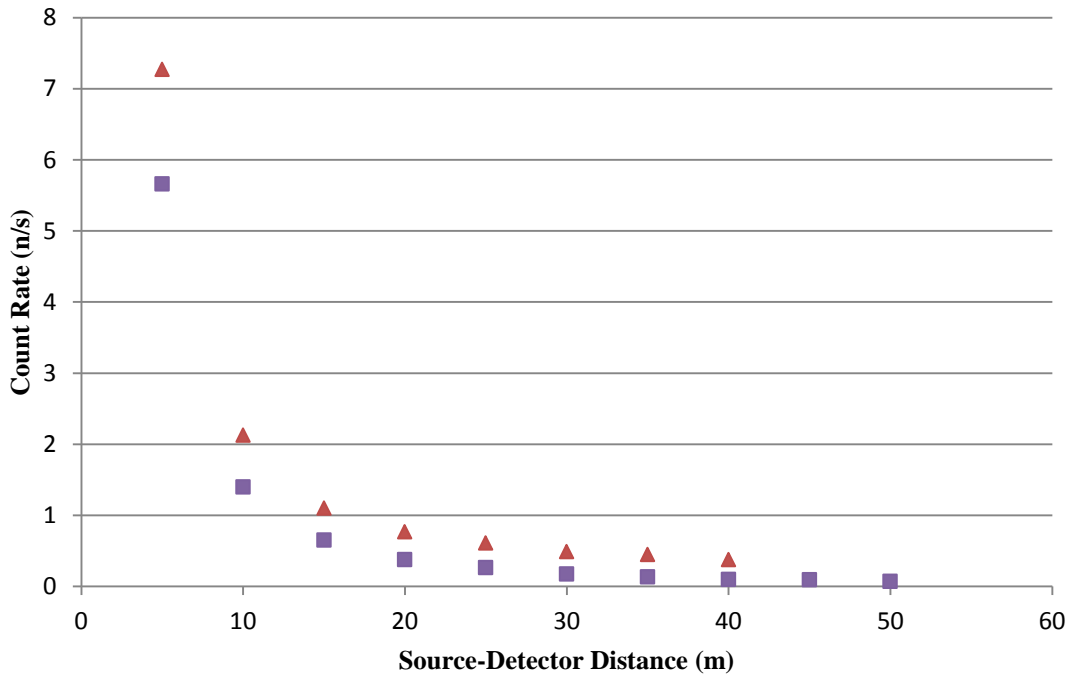


Figure 13. Detector C: Experimental data (triangles) compared with MCNPX modeling (squares) with varying source-detector distances over asphalt

The outputs from MCNPX were analyzed to determine dose rate and count rate for each detector. The MCNPX F4 tally provided dose rate per starting particle in the active Helium-3 cell(s) of the detector which was multiplied by the activity of the source to provide the dose rate; dose rates are summarized in Appendices IV and V. The number of collisions in the active cell(s) of Helium-3 were provided by MCNPX and multiplied by the activity of the source to calculate modeled count rate. The count rates were modeled for all 5 detectors with varying ground type, ground moisture, air moisture, barometric pressure and source-detector distance. The MCNPX modeling results for environmental variables are shown in Figures 14 through 18 and summarized in Appendix VI; modeled count rates are plotted on the ordinate and the variables are plotted on the abscissa for each detector. The count rates for each detector modeled by MCNPX with a source-detector distance of 20 meters did not vary significantly, as seen in Figure 14 through 16, when levels of ground moisture, air moisture, and barometric pressure were changed.

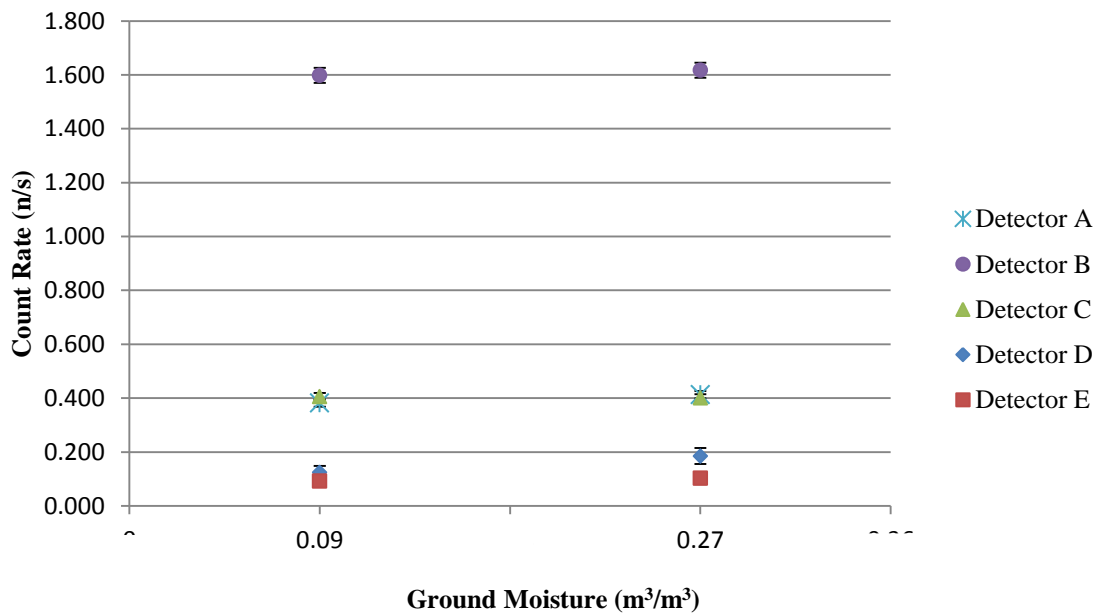


Figure 14. Results of MCNPX modeling with varying ground moisture

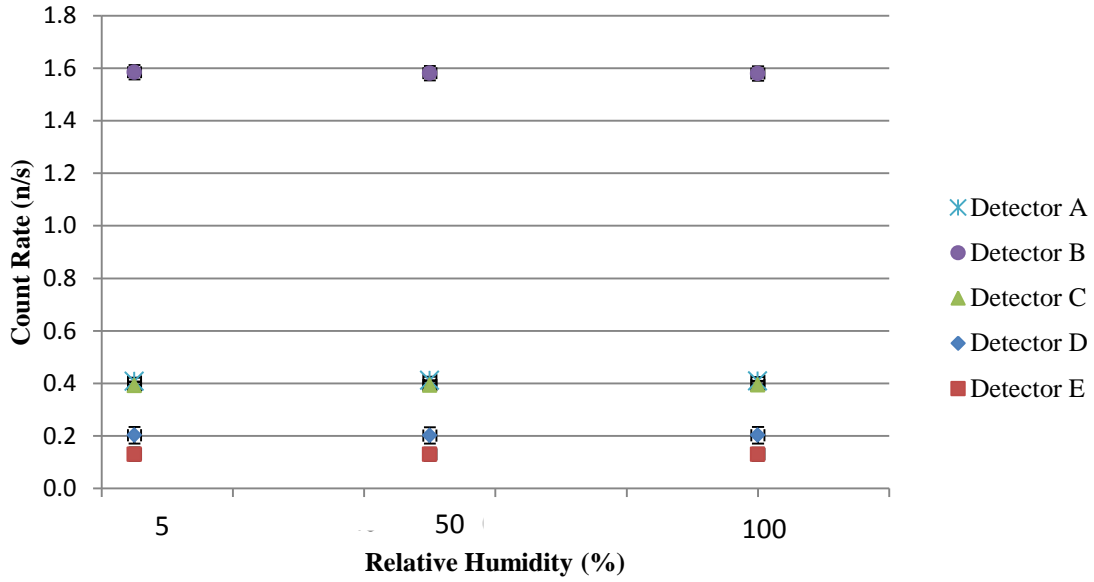


Figure 15. Results of MCNPX modeling with varying air moisture

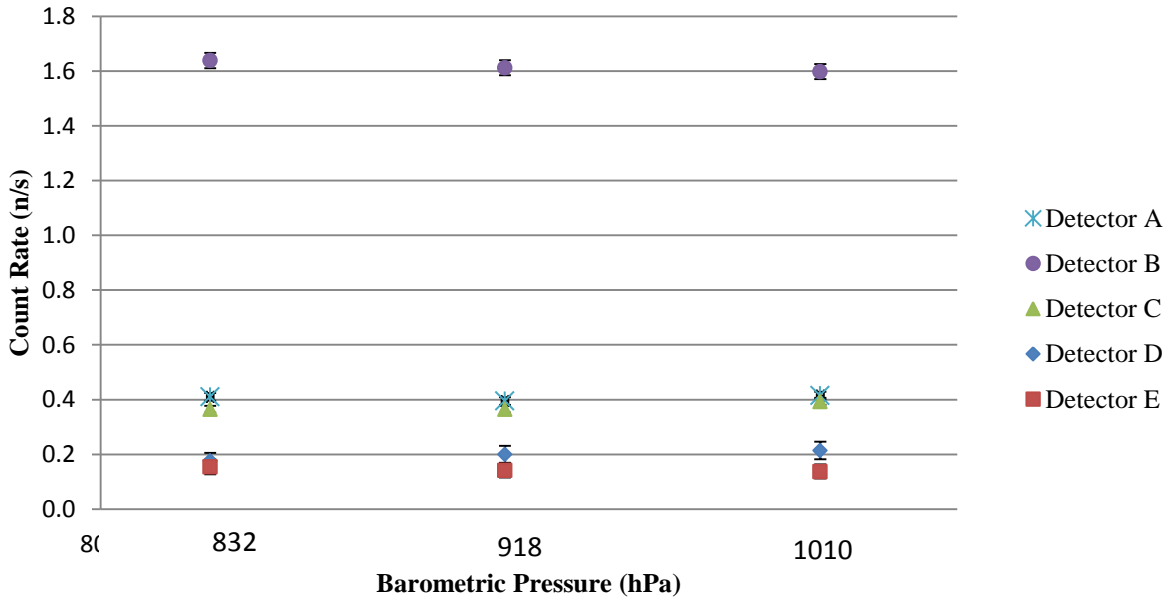


Figure 16. Results of MCNPX modeling with varying barometric pressure

The modeled count rates for the simple detectors had larger variation when the type of ground was changed compared to the complex detectors, as seen in Figures 17 and 18; the source-detector distance modeled was 20 m for all detectors. Experimental results for Detectors

B and C were compared to modeled data for asphalt and soil over a range of source-detector distances, as shown in Figure 19. Experimental and modeled data for Detectors B and C indicate the count rate for these detectors is not affected by the type of ground.

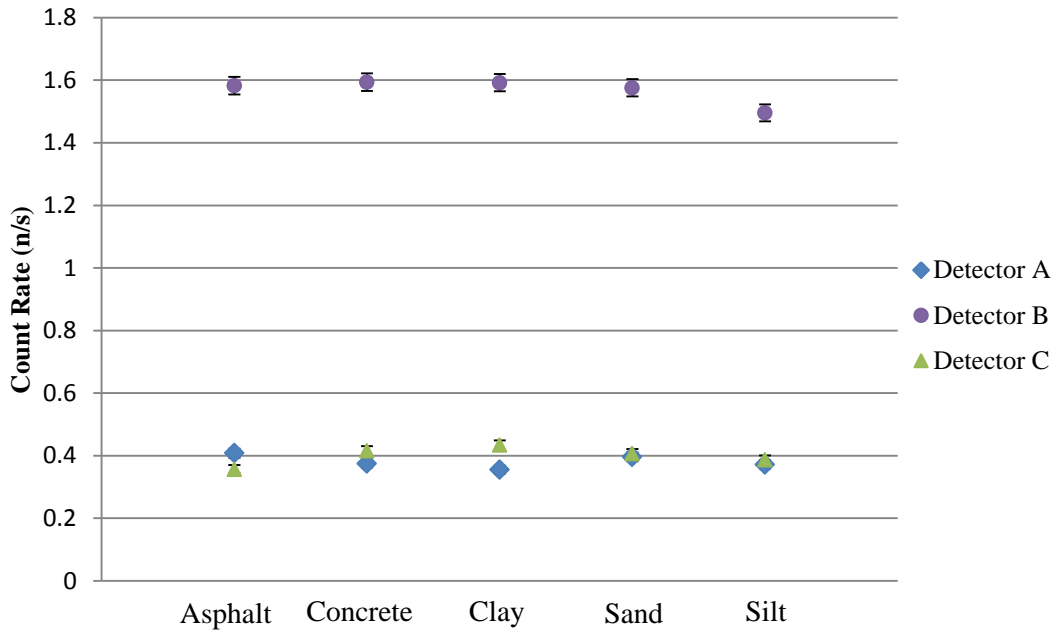


Figure 17. Results of MCNPX modeling with varying ground type for complex detectors

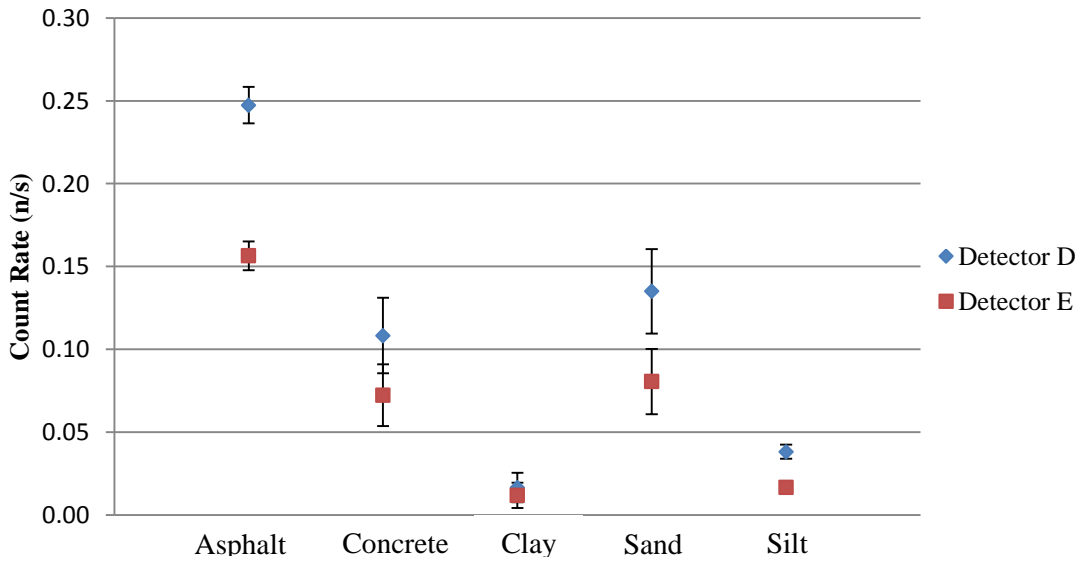


Figure 18. Results of MCNPX modeling with varying ground type for simple detectors

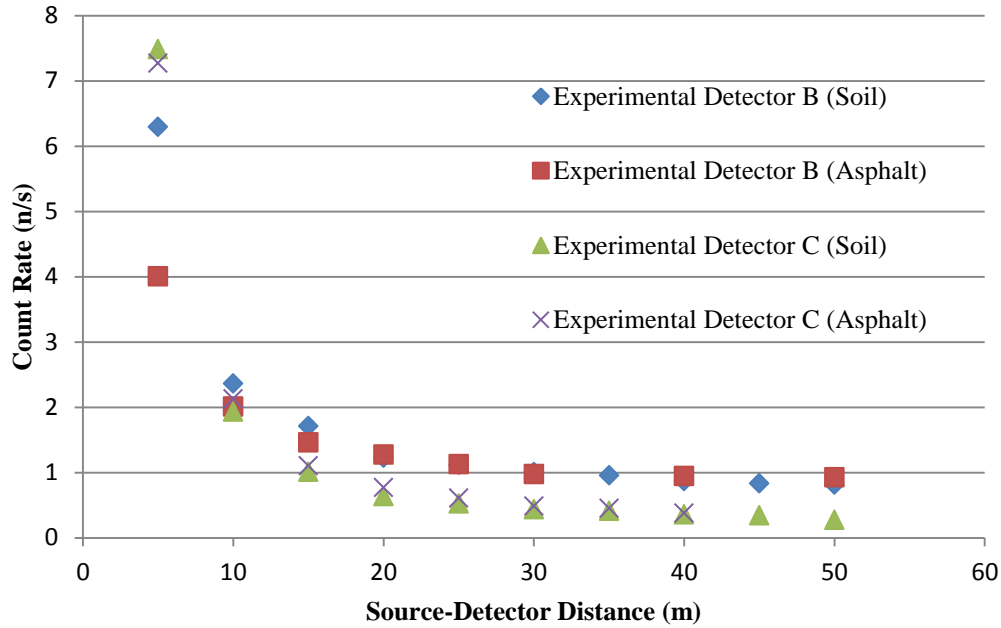


Figure 19. Comparison of effects of ground type for experimental data

As shown in Figure 20 and 21, the count rate decreases with increasing source-detector distance; results are summarized in Appendix VII. The relation between the source-detector distance and how it compares to the “ $1/R^2$  Law” is summarized in Table 9 for Detectors B and C experimental and modeled results; the expected exponent for the functional fit is 2 for perfect correspondence with the “ $1/R^2$  Law.” The total number of collisions detected was compared to the number of collisions caused by neutrons that were scattered from the ground at two distances for Detector B; results are summarized in Table 10. Additionally, experimental data collected with moderated sources and detectors were compared to the “ $1/R^2$  Law” to evaluate the effects of moderation on count rate; results are summarized in Tables 11 and 12.

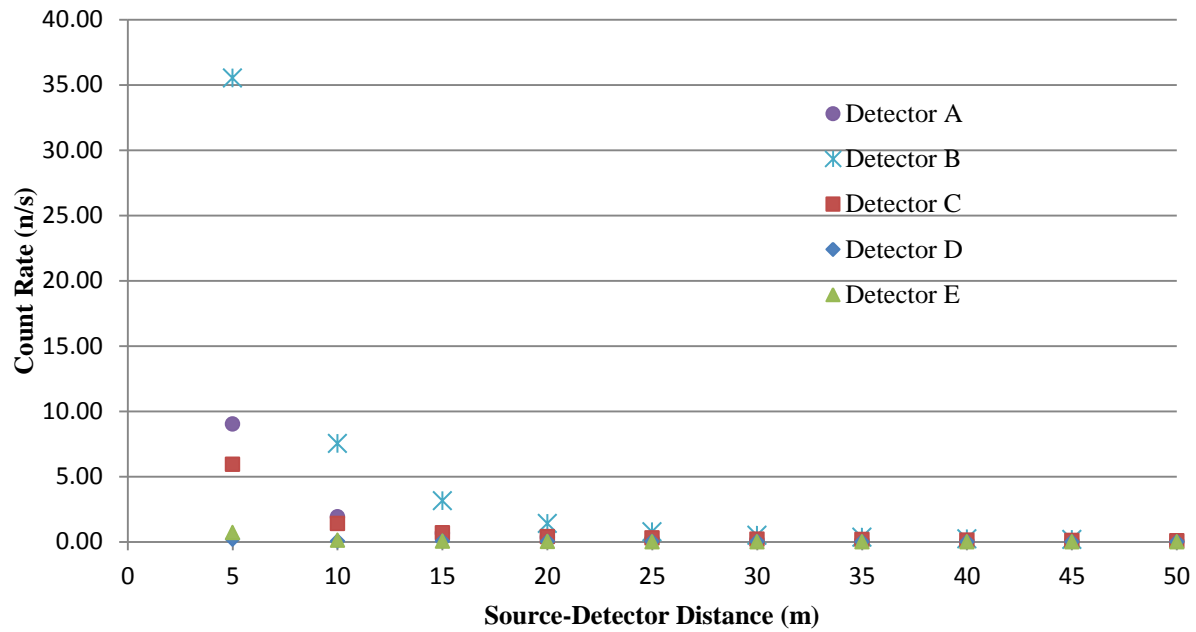


Figure 20. Results of MCNPX modeling with varying source-detector distance over soil

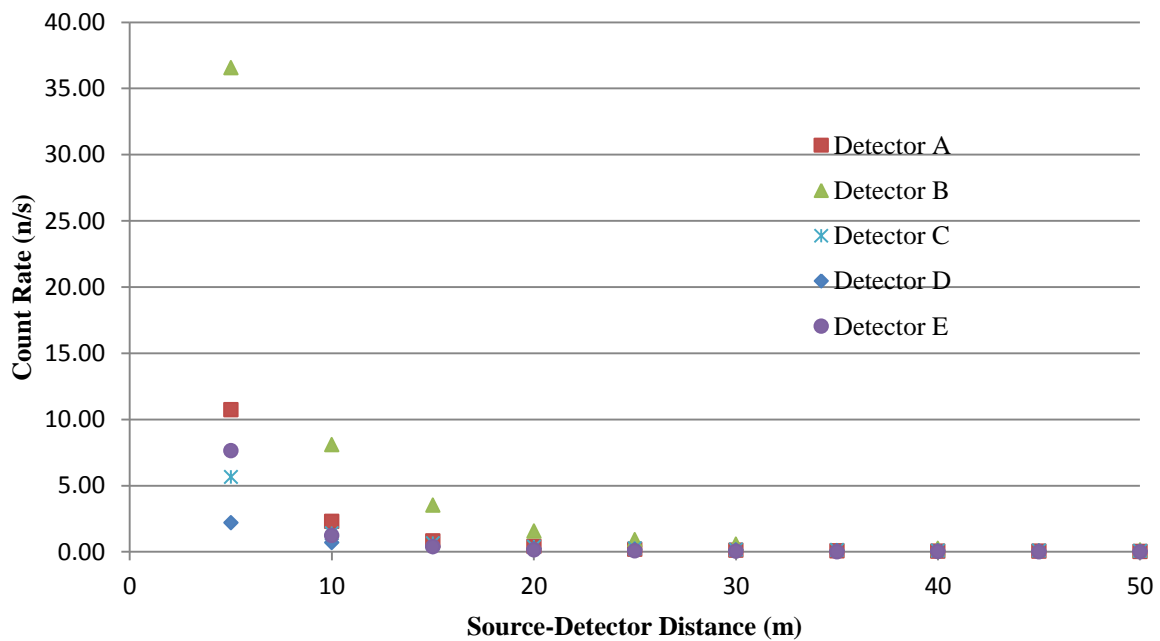


Figure 21. Results of MCNPX modeling with varying source-detector distance over asphalt

**Table 9. Comparison to “1/R<sup>2</sup> Law”**

	<b>Asphalt</b>		<b>Soil</b>	
	1/R <sup>x</sup>	R <sup>2</sup> (curve fit)	1/R <sup>x</sup>	R <sup>2</sup> (curve fit)
<b>Experimental Detector B</b>	0.638	0.9373	0.848	0.9474
<b>Detector B</b>	2.387	0.9975	2.450	0.9979
<b>Experimental Detector C</b>	1.400	0.9830	1.357	0.9647
<b>Detector C</b>	1.885	0.9986	1.806	0.9966

**Table 10. MCNPX modeling data for Detector B**

	<b>Source-detector distance (m)</b>	
	5	10
<b>Total collisions</b>	7798	1653
<b>Collisions from ground</b>	143	28
<b>Ratio</b>	0.018	0.017

**Table 11. Comparison to “1/R<sup>2</sup> Law” with Detector and Source Moderation for Detector B Experimental Results**

<b>Environmental Detector B: 1/R<sup>x</sup></b>			
Detector/Source Moderation	Asphalt	Detector/Source Moderation	Soil
None/Poly	1.447	None/Poly	1.354
1-inch HDPE/Poly	1.264	Poly/Poly	1.249
2-inch HDPE/Poly	1.341		
1-inch HDPE/None	0.981	Poly/None	1.054
None/None	0.638	None/None	0.848

**Table 12. Comparison to “1/R<sup>2</sup> Law” with Source Moderation for Detector C Experimental Results**

<b>Environmental Detector C: 1/R<sup>x</sup></b>			
Detector/Source Moderation	Asphalt	Detector/Source Moderation	Soil
Poly/Poly	1.521	Poly/Poly	1.077
Poly/None	1.400	Poly/None	1.357

## DISCUSSION

As shown in Figure 10 and 11, modeled detector responses were consistently higher than experimental results obtained using Detector B. The higher responses are potentially due to neutron interactions that might not transfer sufficient energy to a charged particle, the proton, which causes the response in the detector. In contrast, modeled count rates for Detector C were consistently lower than experimental measurements, as shown in Figure 12 and 13. The modeling data for Detector C was more consistent with experimental measurements than for Detector B. There are two main differences between Detectors B and C; Detector C has one active Helium-3 tube versus five active cells in Detector B and Detector C has built-in HDPE moderation.

As the amount of moisture in the air or ground increases, the neutron count rate is expected to increase as more fast neutrons are moderated and therefore, detected. However, as shown in Figures 14 and 15, varying moisture content in air or soil has minimal impact on detector response. Varying barometric pressure also had little impact on detector response, as shown in Figure 16 **Error! Reference source not found.**, which was expected since the difference in air composition between 0 and 1609 meters is very small.

Loose, porous soils such as silt and clay loams have more pore space than sandy soils; therefore, silt and clay loams have a lower bulk density. The increased pore space provides increased opportunity for water and therefore, more moderation of neutrons. Therefore, higher neutron count rates are expected for lower density materials. However, as shown in Figure 17 and 18, lower bulk density does not correspond to a higher neutron count rate.

MCNPX modeling results indicate the complex detectors are less affected by changes in the type of ground compared to the simple detectors, as shown in Figure 17 and 18, respectively.

As shown in Figure 18, asphalt had the highest count rate for Detectors D and E, indicating asphalt is more likely to moderate fast neutrons, causing them to scatter; the scattered thermal neutrons may be detected which increases the count rate. Asphalt is comprised of 10% hydrogen, an effective moderator of fast neutrons, which corresponds to the higher count rate. Sand and concrete have less than 1% hydrogen composition, which is more than clay or silt, and corresponds to higher modeled count rates than clay or silt and lower modeled count rates than asphalt, as shown in Figure 18.

Results shown in Figure 17 and 18 indicate the casing and additional components of the complex detectors may provide shielding of scattered neutrons, resulting in less of an effect on count rate with changes in ground material. Additionally, the built-in moderation of Detector C could minimize the effects to count rate with different ground compositions by shielding the scattered thermal neutrons from the ground. The modeling results are supported by experimental data shown in Figure 19 which indicate minimal difference in count rates between asphalt and soil for Detectors B and C.

As shown in Figure 17 and 18, the count rates for Detectors B and E, which have five active Helium-3 tubes, are not five times greater than Detectors C and D which have one Helium-3 tube, as expected. A thorough review of the model data did not provide an unambiguous explanation at this time.

The neutron count rate ( $\dot{R}$ ) is expected to decrease in accordance with the “1/R<sup>2</sup> Law” as the distance ( $d$ ) between the source and detector increases, as shown in Equation 5,

$$\dot{R}_2 = \frac{\dot{R}_1 d_1^2}{d_2^2}. \quad (5)$$

The neutron count rate decreases with increasing source-detector distance, however, not as the “1/R<sup>2</sup> Law” predicts as shown in Table 9. The modeled data is closer to 1/R<sup>2</sup> than the

experimental data collected with Detectors B and C; however, the experimental data more closely follow expected results for Detector C which contains a layer of 3.81-inch HDPE surrounding the Helium-3 tube. The lower count rates than expected at close distances suggest the detector is missing some neutrons, such as fast neutrons that have not been moderated. The MCNP modeling approach selected by this research team accounts for all neutron interactions, including fast neutrons, which could lead to higher count rates than the experimental detector is able to detect.

The ratio of the total number of collisions being detected by Detector B compared to the number of collisions caused by scattered neutrons from the ground was analyzed using a MCNP cell flagging function. As shown in Table 10, the collision ratios at 5 and 10 m are very similar which seems to indicate the difference between modeled and experimental data is not due to the moderated neutrons that are scattered from the ground. Therefore, the data suggest Detector B has lower detection efficiency for fast neutrons from the source at smaller source-detector distances.

Experimental data were also collected with variations of source and detector moderation to determine if moderators increase detection efficiency; the results are summarized in Table 11 and 12. The results indicate moderation of the source has the largest impact on increasing the efficiency of detecting neutrons with smaller source-detector distances for Detector B. However, moderating the source has less of an impact on Detector C which is expected because Detector C is moderated with HDPE. Additional MCNP modeling with moderated source and detector combinations should be completed to compare to experimental results.

## CONCLUSION

Ground composition appears to affect the count rate of simple detectors but does not have an impact on complex detectors, possibly due to the presence of moderating materials. As the percentage of hydrogen in the ground increases, an increased count rate is observed for modeled Detectors D and E, indicating the hydrogen is moderating fast neutrons which are then being detected. Experimental and modeled neutron count rates for Detectors B and C indicate the complex detectors provide enough shielding to prevent scattered thermal neutrons from being detected; therefore, the count rate of the complex detectors is not affected by changes in ground composition.

Based on MCNPX modeling, different levels of moisture in the air or ground do not appear to impact the count rate for the detectors modeled. Changes in barometric pressure, in relation to changes in elevation, do not impact detector response.

Experimental and modeled data using MCNPX show decreasing count rate with increasing source-detector distance; however, the experimental data collected do not follow the “ $1/R^2$  Law” as predicted and should be further analyzed. Using moderated sources and detectors to collect additional experimental data will provide information regarding detection of fast and thermal neutrons; experimental results should be compared to MCNPX modeling results.

## REFERENCES

- Bahadori, A. H. (2011). Estimation of saturated air water content at elevated pressures using simple predictive tool. *Chemical Engineering Research and Design*, 179-186.
- Bevington, P. R. (2003). *Data Reduction and Error Analysis for the Physical Sciences*. New York: McGraw-Hill.
- Cember, H. a. (2009). *Introduction to Health Physics*. New York: McGraw-Hill.
- Crane, T.W. and Baker, M.P. (1991). Neutron Detectors. In *Passive Nondestructive Assay of Nuclear Materials*. Los Alamos.
- D. Mazed, S. M. (2012). Design parameters and technology optimization of <sup>3</sup>He-filled proportional counters for thermal neutron detection and spectrometry applications. *Radiation Measurements*, 577-587.
- European Space Agency. (2012). *Climate Change Initiative*. Retrieved February 3, 2014, from <http://www.esa-soilmoisture-cci.org>
- European Space Agency. (2012). *Product Specification Document (PSD) Version 0.3*.
- Ide, K. e. (2012). Analysis of a measured neutron background below 6 MeV for fast-neutron imaging systems. *Nuclear Instruments and Methods in Physics Research A*, 24-31.
- International Standard (ISO/DIS 8529-1). (2000). *Reference Neutron Radiations Part 1: Characteristics and Methods of Production*.
- Kalos, M. H. (2008). *Monte Carlo Methods*. WILEY-VCH Verlag GmbH & Co.
- Knoll, G. F. (2010). *Radiation Detection and Measurement*. Hoboken: John Wiley & Sons.
- Pacific Northwest National Laboratory. (2011). *Compendium of Material Composition Data for Radiation Transport Modeling*.
- Remote Sensing Laboratory. (n.d.). Joint Base Andrews.
- Turner, J. E. (2007). *Atoms, Radiation, and Radiation Protection*. KGaA, Weinheim: Wiley-CHH Verlag GmbH & Co.
- Tziaferi, E. (2007). First measurement of low intensity fast neutron background from rock at the Boulby Underground Laboratory. *Astroparticle Physics*, 326-338.
- United States Government Accountability Office. (2011). *Neutron Detectors Alternatives to using helium-3*.
- USDA Natural Resources Conservation Service. (2008). *Soil Quality Indicators*.

## APPENDIX I

Californium-252 spontaneous fission source spectra  
(International Standard (ISO/DIS 8529-1), 2000)

$E_i$ (MeV)	$B_i$ (s <sup>-1</sup> )
4.14E-07	3.10E-10
1.00E-06	1.11E-08
1.00E-05	1.27E-07
5.00E-05	2.76E-07
1.00E-04	7.82E-07
2.00E-04	2.21E-06
4.00E-04	4.53E-06
7.00E-04	5.68E-06
1.00E-03	5.51E-05
3.00E-03	1.28E-04
6.00E-03	2.30E-04
1.00E-02	7.74E-04
2.00E-02	2.17E-03
4.00E-02	2.80E-03
6.00E-02	3.29E-03
8.00E-02	3.68E-03
1.00E-01	1.05E-02
1.50E-01	1.21E-02
2.00E-01	1.33E-02
2.50E-01	1.42E-02
3.00E-01	1.49E-02
3.50E-01	1.55E-02
4.00E-01	1.60E-02
4.50E-01	1.63E-02
5.00E-01	1.66E-02
5.50E-01	1.68E-02
6.00E-01	3.38E-02
7.00E-01	3.39E-02
8.00E-01	3.37E-02
9.00E-01	3.33E-02
1.00E+00	6.46E-02
1.20E+00	6.12E-02
1.40E+00	5.73E-02
1.60E+00	5.31E-02
1.80E+00	4.88E-02
2.00E+00	6.55E-02
2.30E+00	5.67E-02
2.60E+00	6.33E-02
3.00E+00	6.21E-02
3.50E+00	4.68E-02

---

4.00E+00	3.49E-02
4.50E+00	2.58E-02
5.00E+00	3.30E-02
6.00E+00	1.74E-02
7.00E+00	9.01E-03
8.00E+00	4.61E-03
9.00E+00	2.33E-03
1.00E+01	1.17E-03
1.10E+01	5.83E-04
1.20E+01	2.88E-04
1.30E+01	1.42E-04
1.40E+01	6.94E-05

---

APPENDIX II

(Pacific Northwest National Laboratory, 2011)

<b>Soil Type: Clay</b>		
<b>Element</b>	<b>Neutron ZA</b>	<b>Weight Fraction</b>
<b>O</b>	8016	0.484345
<b>Na</b>	11023	0.007608
<b>Mg</b>	12000	0.010691
<b>Al</b>	13027	0.122125
<b>Si</b>	14000	0.294194
<b>P</b>	15031	0.000113
<b>K</b>	19000	0.020427
<b>Ca</b>	20000	0.018957
<b>Ti</b>	22000	0.004668
<b>Mn</b>	25055	0.000064
<b>Fe</b>	26000	0.036804

<b>Soil Type: Soil (Earth), U.S. Average</b>		
<b>Element</b>	<b>Neutron ZA</b>	<b>Weight Fraction</b>
<b>O</b>	8016	0.513713
<b>Na</b>	11023	0.006140
<b>Mg</b>	12000	0.013303
<b>Al</b>	13027	0.068563
<b>Si</b>	14000	0.271183
<b>K</b>	19000	0.014327
<b>Ca</b>	20000	0.051167
<b>Ti</b>	22000	0.004605
<b>Mn</b>	25055	0.000716
<b>Fe</b>	26000	0.056283

<b>Soil Type: Sand</b>		
<b>Element</b>	<b>Neutron ZA</b>	<b>Weight Fraction</b>
<b>H</b>	1001	0.007833
<b>C</b>	6000	0.003360
<b>O</b>	8016	0.536153
<b>Na</b>	11023	0.017063
<b>Al</b>	13027	0.034401
<b>Si</b>	14000	0.365067
<b>K</b>	19000	0.011622
<b>Ca</b>	20000	0.011212
<b>Fe</b>	26000	0.013289

### APPENDIX III

(Pacific Northwest National Laboratory, 2011)

<b>Ground Type: Asphalt</b>		
<b>Element</b>	<b>Neutron ZA</b>	<b>Weight Fraction</b>
<b>H</b>	1001	0.103725
<b>C</b>	6000	0.848050
<b>N</b>	7014	0.006050
<b>O</b>	8016	0.004050
<b>S</b>	16000	0.037700
<b>V</b>	23000	0.000393
<b>Ni</b>	28000	0.000034

<b>Ground Type: Concrete, Los Alamos (MCNP)</b>		
<b>Element</b>	<b>Neutron ZA</b>	<b>Weight Fraction</b>
<b>H</b>	1001	0.004530
<b>O</b>	8016	0.512600
<b>Na</b>	11023	0.015270
<b>Al</b>	13027	0.035550
<b>Si</b>	14000	0.360360
<b>Ca</b>	20000	0.057910
<b>Fe</b>	26000	0.013780

APPENDIX IV

Summary of dose rates with varying environmental conditions

	Detector A		Detector B		Detector C		Detector D		Detector E	
Ground Type	Dose Rate ( $\frac{\mu\text{rem}}{h}$ )	Unc* (%)	Dose Rate ( $\frac{\mu\text{rem}}{h}$ )	Unc (%)						
Asphalt	10.55	1.22	18.66	0.77	0.91	2.85	1.63	1.68	1.42	0.81
Concrete	10.93	1.20	19.33	0.75	0.99	2.71	1.84	1.60	1.52	1.44
Clay	11.10	1.19	19.56	0.75	1.03	2.64	1.92	1.57	1.55	0.05
Sand	10.79	1.20	19.21	0.75	0.98	2.72	1.78	1.63	1.52	0.05
Silt	11.23	1.18	18.70	0.76	1.01	2.66	1.97	1.54	1.46	0.78

	Detector A		Detector B		Detector C		Detector D		Detector E	
Ground Moisture (m <sup>3</sup> /m <sup>3</sup> )	Dose Rate ( $\frac{\mu\text{rem}}{h}$ )	Unc* (%)	Dose Rate ( $\frac{\mu\text{rem}}{h}$ )	Unc (%)						
0.09	10.77	1.20	19.20	0.76	0.97	2.74	1.80	1.62	1.51	0.05
0.27	10.59	1.22	18.86	0.76	0.92	2.80	1.70	1.66	1.46	0.05

	Detector A		Detector B		Detector C		Detector D		Detector E	
Air Moisture (% RH)	Dose Rate ( $\frac{\mu\text{rem}}{h}$ )	Unc* (%)	Dose Rate ( $\frac{\mu\text{rem}}{h}$ )	Unc (%)						
5	10.55	1.22	18.65	0.77	0.92	2.80	1.65	1.70	1.44	0.05
50	10.53	1.22	18.66	0.77	0.92	2.80	1.65	1.70	1.44	0.05
100	10.52	1.22	18.64	0.77	0.92	2.80	1.65	1.69	1.44	0.05

	Detector A		Detector B		Detector C		Detector D		Detector E	
Barometric Pressure (hPa)	Dose Rate ( $\frac{\mu\text{rem}}{h}$ )	Unc* (%)	Dose Rate ( $\frac{\mu\text{rem}}{h}$ )	Unc (%)						
1010	10.60	1.22	18.81	0.77	0.92	2.82	1.64	1.68	1.45	0.05
918	10.71	1.22	19.13	0.76	0.95	2.77	1.65	1.69	1.45	0.05
832	10.77	1.21	19.25	0.76	0.93	2.80	1.63	1.70	1.47	0.05

\*Uncertainty

APPENDIX V

Summary of dose rates with varying source-detector distances

Asphalt										
Source-Detector Distance (m)	Detector A		Detector B		Detector C		Detector D		Detector E	
	Dose Rate ( $\frac{\mu\text{rem}}{h}$ )	Unc* (%)	Dose Rate ( $\frac{\mu\text{rem}}{h}$ )	Unc (%)	Dose Rate ( $\frac{\mu\text{rem}}{h}$ )	Unc (%)	Dose Rate ( $\frac{\mu\text{rem}}{h}$ )	Unc (%)	Dose Rate ( $\frac{\mu\text{rem}}{h}$ )	Unc (%)
5	207.01	0.28	364.77	0.55	15.62	2.16	25.75	0.43	25.39	0.61
10	49.43	0.57	86.73	1.13	3.86	4.31	6.67	0.84	6.26	1.22
15	20.63	0.88	36.22	1.74	1.68	2.12	2.96	1.25	2.62	1.90
20	10.55	1.22	18.66	0.77	0.91	2.85	1.63	1.68	1.42	0.81
25	6.02	0.51	11.00	1.00	0.60	3.53	1.06	2.11	0.83	1.05
30	3.84	0.64	7.09	1.23	0.38	4.36	0.68	2.59	0.55	1.30
35	2.61	0.78			0.29	5.07	0.53	2.97		
40	1.91	2.82	3.45	1.76	0.20	5.82	0.37	3.54	0.28	1.83
45	1.43	3.32			0.18	6.26	0.28	4.03	0.21	2.13
50	1.04	3.72	1.96	2.32	0.13	7.60	0.23	4.37	0.15	2.45

Silt										
Source-Detector Distance (m)	Detector A		Detector B		Detector C		Detector D		Detector E	
	Dose Rate ( $\frac{\mu\text{rem}}{h}$ )	Unc* (%)	Dose Rate ( $\frac{\mu\text{rem}}{h}$ )	Unc (%)	Dose Rate ( $\frac{\mu\text{rem}}{h}$ )	Unc (%)	Dose Rate ( $\frac{\mu\text{rem}}{h}$ )	Unc (%)	Dose Rate ( $\frac{\mu\text{rem}}{h}$ )	Unc (%)
5	234.97	0.80	403.88	0.51	17.32	1.98	30.80	0.39	30.11	0.55
10	51.96	1.69	90.55	1.07	4.09	4.09	7.57	0.77	6.91	1.14
15	20.90	0.84	36.02	1.70	1.80	1.98	3.29	1.16	2.77	1.84
20	10.60	1.18	17.66	0.76	0.95	2.66	1.86	1.54	1.46	0.78
25	6.26	1.54	9.93	1.02	0.61	3.30	1.23	1.91	0.85	1.02
30	3.95	1.94	6.33	1.27	0.41	4.00	0.81	2.30	0.55	1.27
35	2.68	2.32	4.31	1.53	0.31	4.61	0.61	2.66	0.38	1.52
40	1.90	2.74	3.11	1.82	0.23	5.21	0.47	3.08	0.28	1.79
45	1.41	3.21	2.23	2.10	0.19	5.68	0.35	3.52	0.20	2.08
50	1.06	3.66			0.14	6.94	0.27	3.90	0.15	2.40

\*Uncertainty

APPENDIX VI

Summary of neutron count rates with varying environmental conditions

	Detector A		Detector B		Detector C		Detector D		Detector E	
Ground Type	Count Rate (n/s)	Unc* (%)	Count Rate (n/s)	Unc (%)						
Asphalt	0.408	1.40	1.58	2.76	0.357	1.35	0.247	1.09	0.156	0.87
Concrete	0.375	1.35	1.59	2.77	0.416	1.42	0.108	2.29	0.072	1.87
Clay	0.355	1.31	1.59	2.77	0.434	1.45	0.016	0.89	0.012	0.75
Sand	0.397	1.38	1.58	2.76	0.407	1.40	0.135	2.55	0.081	1.97
Silt	0.372	1.34	1.50	2.69	0.387	1.41	0.038	0.43	0.017	0.28

	Detector A		Detector B		Detector C		Detector D		Detector E	
Ground Moisture (m <sup>3</sup> /m <sup>3</sup> )	Count Rate (n/s)	Unc* (%)	Count Rate (n/s)	Unc (%)						
0.09	0.381	1.36	1.60	2.78	0.406	1.32	0.124	2.45	0.092	2.10
0.27	0.413	1.41	1.62	2.79	0.401	1.31	0.185	2.99	0.102	2.22

	Detector A		Detector B		Detector C		Detector D		Detector E	
Air Moisture (% RH)	Count Rate (n/s)	Unc* (%)	Count Rate (n/s)	Unc (%)						
5	0.408	1.40	1.58	2.76	0.392	1.30	0.203	3.13	0.131	2.51
50	0.412	1.41	1.58	2.76	0.394	1.30	0.202	3.12	0.130	2.51
100	0.410	1.41	1.58	2.76	0.395	1.30	0.203	3.13	0.131	2.51

	Detector A		Detector B		Detector C		Detector D		Detector E	
Barometric Pressure (hPa)	Count Rate (n/s)	Unc* (%)	Count Rate (n/s)	Unc (%)						
1010	0.415	1.41	1.60	2.78	0.393	1.30	0.214	3.21	0.138	2.58
918	0.395	1.38	1.61	2.79	0.365	1.25	0.200	3.11	0.142	2.62
832	0.410	1.41	1.64	2.81	0.365	1.25	0.177	2.92	0.154	2.73

\*Uncertainty

APPENDIX VII

Summary of neutron count rates with varying source-detector distances

<b>Asphalt</b>					
<b>Source-Detector Distance (m)</b>	<b>Detector A</b>		<b>Experimental Detector B</b>	<b>Detector B</b>	
	<b>Count Rate (n/s)</b>	<b>Unc* (%)</b>	<b>Count Rate (n/s)</b>	<b>Count Rate (n/s)</b>	<b>Unc (%)</b>
<b>5</b>	10.73	22.75	4.00	36.58	42.00
<b>10</b>	2.30	10.54	2.01	8.10	19.77
<b>15</b>	0.83	6.34	1.46	3.52	13.04
<b>20</b>	0.41	1.40	1.28	1.58	2.76
<b>25</b>	0.20	0.31	1.13	0.92	0.67
<b>30</b>	0.13	0.25	0.98	0.59	0.53
<b>35</b>	0.08	0.20			
<b>40</b>	0.06	0.53	0.94	0.28	0.36
<b>45</b>	0.04	0.45			
<b>50</b>	0.03	0.38	0.93	0.15	0.86

<b>Asphalt</b>							
<b>Source-Detector Distance (m)</b>	<b>Experimental Detector C</b>	<b>Detector C</b>		<b>Detector D</b>		<b>Detector E</b>	
	<b>Count Rate (n/s)</b>	<b>Count Rate (n/s)</b>	<b>Unc* (%)</b>	<b>Count Rate (n/s)</b>	<b>Unc (%)</b>	<b>Count Rate (n/s)</b>	<b>Unc (%)</b>
<b>5</b>	7.27	5.66	16.53	2.21	3.26	7.64	19.20
<b>10</b>	2.13	1.40	8.22	0.69	1.83	1.24	7.73
<b>15</b>	1.10	0.65	1.78	0.38	1.36	0.38	4.30
<b>20</b>	0.77	0.38	1.35	0.25	1.09	0.16	0.87
<b>25</b>	0.61	0.27	1.13	0.19	0.95	0.08	0.62
<b>30</b>	0.49	0.18	0.92	0.14	0.83	0.04	0.44
<b>35</b>	0.45	0.13	0.80	0.11	0.72	0.00	0.00
<b>40</b>	0.38	0.10	0.69	0.09	0.64	0.01	0.27
<b>45</b>		0.09	0.67	0.06	0.54	0.01	0.21
<b>50</b>		0.07	0.59	0.06	0.53	0.01	0.20

\*Uncertainty

Silt					
Source-Detector Distance (m)	Detector A		Experimental Detector B	Detector B	
	Count Rate (n/s)	Unc* (%)	Count Rate (n/s)	Count Rate (n/s)	Unc (%)
5	9.03	21.48	6.29	35.51	40.2
10	1.91	9.88	2.36	7.53	18.5
15	0.67	1.85	1.71	3.15	12.0
20	0.35	1.34	1.22	1.41	2.5
25	0.20	1.01	1.12	0.77	1.9
30	0.14	0.83	1.01	0.49	1.5
35	0.08	0.64	0.96	0.35	1.3
40	0.05	0.50	0.87	0.23	1.0
45	0.04	0.45	0.84	0.17	0.9
50	0.03	0.36	0.81		

Silt							
Source-Detector Distance (m)	Experimental Detector C	Detector C		Detector D		Detector E	
	Count Rate (n/s)	Count Rate (n/s)	Unc* (%)	Count Rate (n/s)	Unc (%)	Count Rate (n/s)	Unc (%)
5	7.49	5.94	16.4	0.20	0.9	0.72	5.7
10	1.93	1.40	8.0	0.06	0.5	0.12	2.4
15	1.01	0.70	1.8	0.04	0.4	0.05	1.5
20	0.64	0.39	1.3	0.04	0.4	0.02	0.3
25	0.53	0.30	1.2	0.02	0.3	0.01	0.2
30	0.44	0.20	1.0	0.02	0.3	0.00	0.1
35	0.41	0.16	0.9	0.01	0.2	0.00	0.1
40	0.36	0.12	0.7	0.01	0.2	0.00	0.1
45	0.34	0.11	0.7	0.01	0.2	0.00	0.1
50	0.27	0.09	0.6	0.01	0.2	0.00	0.0

\*Uncertainty